https://doi.org/10.1016/j.compscitech.2021.108747

An Implantable, Compatible and Networkable Nanocomposite Piezoresistive Sensor for *in situ* Acquisition of Dynamic Responses of CFRPs

Yiyin Su[a], Jianwei Yang[a], Yaozhong Liao[a], Pengyu Zhou[a], Lei Xu[a],
Li-min Zhou[b] and Zhongqing Su[a,c,d*]

[a] Department of Mechanical Engineering,
The Hong Kong Polytechnic University, Kowloon, Hong Kong SAR

[b] School of System Design and Intelligent Manufacturing,
Southern University of Science and Technology, Shenzhen 518055, PR China

[c] The Hong Kong Polytechnic University Shenzhen Research Institute, Shenzhen 518057, P.R. China

[d] School of Astronautics, Northwestern Polytechnical University, Xi'an, 710072, P.R. China

submitted to ***Composites Science and Technology***
(initially submitted on 29 Oct 2020; revised and re-submitted on 24 Jan 2021)

[*] To whom correspondence should be addressed. Tel.: +852-2766-7818, Fax: +852-2365-4703,
Email: zhongqing.su@polyu.edu.hk (Prof. Zhongqing Su, *Ph.D.*)

Abstract

When sensors are embedded in composites for structural integrity monitoring (SIM), the sensors *per se*, unfortunately, degrade the original integrity of host composites. Envisaging such deficiency and facilitated by advances in nanotechnology, we develop a new type of ultrathin, piezoresistive sensors using spraying coating and nanocomposites formulated with graphene nanoplatelets/polyvinylpyrrolidone. The sensors are deposited on dielectric membranes made of partially pre-cured B-stage epoxy films, then electrified using carbon nanotube film (CNT-film)-made wires, and implanted in carbon fibre-reinforced polymer composites (CFRPs), to form a sensor network. Only ~45 μm thick (including wires), the implanted sensors exhibit high compatibility and nonintrusive attributes with CFRPs, enabling composites to perceive broadband signals *in situ*, ranging from static strain (with a high gauge factor of 34.5) to structure-guided ultrasonic waves up to 450 kHz – the first time that piezoresistive sensors implanted in CFRPs respond to dynamic strains in such a broad frequency band. CFRPs with implanted sensor networks are endowed with capacity of *in situ* SIM, yet not compromising their original integrity. With remarkably reduced intrusion to composites – as proven in tensile and bending tests, the developed sensors outperform prevailing sensors for SIM of composites such as lead zirconate titanate-based sensors.

Keywords**:** CFRPs; structural health monitoring; implantable nanocomposite sensor; piezoresistive sensor; guided ultrasonic waves

1. Introduction

By virtue of superior mechanical attributes, carbon fibre-reinforced polymer composites (CFRPs) have attained their maturity to serve as primary load-bearing structural components, in lieu of conventional metallic materials [1]. As CFRPs age in service, the structural integrity is degraded progressively, entailing monitoring of structural integrity in a continuous and, preferably, near to a real-time manner. With years of intensive effort, structural integrity monitoring (SIM) has now become an essential building block in the overall development of high-performance CFRPs targeting demanding engineering applications. SIM has proven effectiveness in enhancing the durability of composites, driving down exorbitant maintenance costs, and extending their residual service life. With such recognition, the past two decades have witnessed a diversity of SIM techniques that are tailored for CFRPs [2-5].

As the most rudimentary yet pivotal element in SIM, sensors (or elaborately configured sensor networks) are integrated with CFRPs, for capturing ambient variations and structural changes, on which basis material degradation or structural damage such as fibre breakage, impact-induced delamination or matrix cracking can be characterized via appropriate physical models and searching algorithms. Prevailing sensors that can be used to fulfill SIM for composites broadly embrace acoustic emission (AE) sensors [6], accelerometers [7], strain gauges [8], fibre Bragg grating (FBG) sensors [9], interdigital transducers (IDTs) [10], polyvinylidene fluoride (PVDF) film sensors [11], lead zirconate titanate (PZT) wafers [12, 13], among others.

Sensors, of whatever kind, are immobilized with CFRPs via either surface mounting [6, 14] or internal embedding [9, 15-17], each possessing respective merits and demerits. Depending on applications, selection of a proper means for sensor immobilization in composites is somewhat debatable. Surface mounting is preferable when the convenience of sensor installation, ease of maintenance, and low replacement cost are priority considerations [18], though it is increasingly challenged due to the inferior accuracy in signal acquisition, because sensors are exposed directly to the environment and prone to ambient noise. This concern is particularly accentuated for CFRPs used in rugged working conditions such as the composite-made load-bearing structures in aircraft.

In contrast to the surface attachment, internal embedment of sensors has advantages when isolation of sensors from the environment is of necessity. As a consequence of the reduced exposure to ambient, the embedded sensors usually offer a high signal-to-noise ratio and enhanced immunity to measurement noise, along with stability, durability and repeatability of long-term signal acquisition. Internal embedding of sensors is also conducive to preventing detachment of sensors from composites due to reasons such as adhesive degradation or environmental attack (*e.g.*, moisture and corrosion). In addition, embedded sensors are in general more sensitive to internal damage than surface attached sensors are [17]. When sensors, as typified by rigid PZT wafers or brittle FBG sensors, are embedded in CFRPs, it is envisaged that the sensors may compromise the integrity of the host composites, regardless of the fact that the intended role of the sensors is to implement integrity monitoring of the CFRPs [19, 20]. To put it into perspective, Konka *et al.* [21] proved that an embedded PZT wafer could reduce the interlaminar shear strength of CFRPs remarkably by up to 15%, and in the meantime observed premature material failure initiated from the PZT wafer edge. This can be attributed to the fact that the significant difference in mechanical properties between PZT materials and CFRPs discontinues the strains at the sensor interface and engenders high stress concentration therein.

In addition to the embedded sensors themselves, the associated wires/cables, electrodes, and the dielectric films such as polyimide (Kapton) [15, 16] that are used to insulate sensors from carbon fibres to prevent short-circuit, also intensify the degradation of structural integrity. The dielectric films, though thin, can alter the microstructure of a fibre-reinforced matrix, influence the interlaminar stress distribution in sensor vicinity, introduce artificial defect, and consequently lower the load-carrying capability of CFRPs. Andreades *et al.* [17] demonstrated that both the flexural and compression strengths of CFRPs decreased by 8% and 12%, respectively, due to embedded transducers coated with polyimide films. Xiao *et al.* [6] examined the influence of embedded metallic materials on tensile properties of CFRPs, to reveal that delamination at the interface between the metal and matrix was a key damage mechanism, implying that embedded metal wires could result in integrity degradation of composites.

Other challenging issues arising from sensor embedding, in comparison with surface mounting, also include the difficulty in precisely placing and aligning sensors in composites during lay-up, the ease in breaking vulnerable cables (used for linking sensors to external acquisition equipment) during edge-trimming, and the impossibility to access or replace embedded sensors during maintenance, along with high manufacturing cost. Furthermore, PZT wafers, rigid and brittle, are inadaptable to a curved structure, while FBG sensors are in generally not sensitive to damage far from their vicinity [22]. Moreover, due to their high sensitivity to moisture and chemicals, FBG sensors need to be protected by polymer sheaths which may introduce localized mechanical weakness in the composites [16]. Together, all these factors can significantly undermine the original integrity of CFRPs due to sensor intrusion, cause premature failure, and jeopardize the use of SIM for enhancing structural reliability.

On the other hand, the recent prosperity in nanotechnology, printed electronics and additive manufacturing has ushered in a promising avenue to substantially downsize sensors, whereby the intrusion to composites might be minimized, along with appealing merits such as reduced producing cost, standardized fabrication procedure, as well as accurate sensor alignment and positioning [23]. As a pioneering study, Thestenson *et al.* [24] dispersed an electrical percolating carbon nanotubes (CNTs) network in glass fibre-reinforced polymer composites (GFRPs), for detecting matrix-dominated failures, revealing that an embedded CNT network inflicted insignificant effect on the integrity of GFRPs. In a similar vein, dip-coating [25], electrophoretic deposition (EPD) [26], or in-situ chemical vapor deposition (CVD) growth [27] were, respectively, used to decorate glass fibres with carbonaceous nanomaterials for sensing purposes, while not at the cost of sacrificing the composites' integrity. Nevertheless, these approaches are usually constrained to polymer composites with dielectric glass fibres, in which the short-circuit of sensors by fibres is not a concern.

To break through such constriction and extend sensor embedding from GFRPs to CFRPs for strain measurement, macroscopic carbon nanotube sheets [28, 29] (also referred to as "buckypaper") are adopted to avoid short-circuit of sensors by carbon fibres. Exemplarily, Boztepe *et al.* [29] used a porous CNTs-enriched buckypaper to monitor damage progression in CFRPs under a uniaxial fatigue load. Analogously, most SIM approaches in this category lie in the premise that damage in composites, if any, can alter, more or less, the electrical impedance measured by the buckypaper. However, in addition to the complex fabrication process and difficulty in controlling the initial electrical properties of the buckypaper, these approaches may fail to provide quantitative evaluation of the degradation (e.g., accurate location and estimate of severity) – that is because the change in electrical impedance only holistically reflects the alteration in material between the two electrodes of the buckypaper – that is global information on the overall change in structural integrity. They may also overlook initial degradation or embryonic damage, because damage of this degree usually incurs unmeasurable shift in electrical conductivity of the buckypaper.

In contrast to scrutinizing global changes in electrical properties, exploration of localized information such as composite structure-guided ultrasonic waves (GUWs) makes quantitative evaluation of integrity degradation possible, thanks to the localized information that GUWs carry and accumulate along wave propagation path. GUWs also offer much higher sensitivity to material degradation of small scale owing to their short wavelengths, compared with those approaches using global information (e.g., electrical impedance). In conventional GUW-based methods [13, 16], piezoelectric sensors (e.g., PZT wafers) are commonly employed to acquire GUWs, which, however, unavoidably threaten the composites' integrity. As far as nanocomposite-based sensors are concerned, although they may not inflict remarkable intrusion on composites, this sort of sensors usually fails to respond to high-frequency GUWs – because GUWs for SIM are of high frequency (of several kHz or even

MHz) yet ultralow magnitude (of the order of micro-strain, even nano-strain) – beyond the responsivity of ordinary nanocomposite-based sensors.

In conclusion, though significance of SIM for CFRPs cannot be overemphasized, it is still a vast challenge to implement continuous SIM in a quantitative manner, but without detrimental impact on composites due to sensor intrusion. Motivated by such recognition and by expanding the authors' continued endeavour in developing nano-engineered sensors for GUW-based structural health monitoring [18, 30-36], this study takes advantage of recent technological advances in nanocomposites and additive manufacturing, aspiring to a new breed of ultrathin, implantable, nano-engineered piezoresistive sensor, capable of perceiving broadband signals and implementing GUW-based SIM for CFRPs, yet without compromising the composites' original integration, mechanical properties and electromechanical performance. The sensors are fabricated using spraying coating and nanocomposites formulated with graphene nanoplatelets (GNPs) and polyvinylpyrrolidone (PVP). With high compatibility and nonintrusive attributes with CFRPs, the implanted sensors enable the composites to perceive broadband signals *in situ*, ranging from static load-induced strain to structure-guided ultrasonic waves. Results are compared with those when PZT wafers are used as sensors. Tensile and bending tests are performed in accordance with ASME standards, to examine possible effect of the implanted sensors on mechanical attributes of CFRPs.

2. Sensor Fabrication and Morphological Characterization

2.1 Sensing Mechanism

GUWs for SIM are often generated in a range from several hundred kilohertz (kHz) to several megahertz (MHz), within which GUWs feature a magnitude of the order of microstrain or even nanostrain. Crucial to faithful acquisition of GUWs is the sensitivity of the sensor material to external disturbance. To endow sensors with sufficient sensitivity to GUWs of high frequencies and ultralow magnitudes, the quantum tunneling effect is exploited. The tunneling effect, a quantum mechanical phenomenon, is triggered at nanoscale in a morphologically proper conductive network, when the insulative barrier among neighbouring conductive nanoparticles are smaller than a critical threshold (of the order of several nanometers in general) [37, 38], under which electrons are able to move through these barriers and consequently induce a tunneling current [39]. The percolation threshold represents a critical fraction of the conductive nanoparticles in the formed network, beyond which a slight increase in the content of conductive nanoparticles can lead to a remarkable leap in the electrical conductivity of the material [40]. Because the barrier to break (so that a tunneling current can be triggered) is of the order of several nanometers only, it is possible for a GUW, even of ultralow magnitude, to alter inter-distances among nanoparticles and activate the tunneling effect, provided the nanoparticle-formed network is morphologically appropriate and the content of conductive nanoparticles is close to the percolation threshold. A triggered tunneling current alters the piezoresistivity manifested by the nanocomposite materials.

Driven by such a quantum tunneling effect-based sensing mechanism, a new type of nanocomposite-based piezoresistive sensor is developed. Upon even dispersion of nanoparticles in matrix, the electrical properties of the synthesized nanocomposites can be calibrated using the percolation theory [40], as

$$\sigma \propto \left(f - f_c \right)^t, \quad \text{when } f > f_c \qquad \textbf{(1)}$$

where σ signifies the electrical conductivity of nanocomposites, f the fraction of nanoparticles, f_c the percolation threshold, and exponential t a constant reflecting the dimensionality of the nanocomposites [37, 38]. The electrical resistance of the sensor (R) embraces three key components: the intrinsic resistance of nanoparticles ($R_{Nanoparticle}$), the contact resistance due to direct contact among nanoparticles ($R_{Contact}$), and the tunneling resistance among nanoparticles (R_{Tunnel}) that is induced by the tunneling effect, namely

$$R = R_{Nanoparticle} + R_{Contact} + R_{Tunnel} \, . \qquad \textbf{(2)}$$

The tunneling effect is particularly prominent when the content of conductive nanoparticles is close to the percolation threshold of the nanoparticle-formed conductive network, and therefore R_{Tunnel} dominates the responsivity of a sensor when the sensor perceives a GUW signal – this is different from the case when the sensor is subject to an external load with a relatively large magnitude (*e.g.*, structural vibration or tensile-induced strain) under which the change in electrical resistance of the sensor is mainly attributed to the breakup of conductive network or loss of contacts among nanoparticles (i.e., change in $R_{Contact}$).

2.2 Fabrication of Implantable Sensors

A specific kind of conductive polymer nanocomposites (CPCs) is prepared as the nanocomposite ink for sensor fabrication using spray coating. The fabricated sensors are further electrified, circuited and networked with highly conductive CNT-film-made wires, to be implanted into CFRPs and form a sensor network.

Synthesis of Nanocomposite Ink

A standard solution mixing process is applied to prepare the sprayable nanocomposite ink. PVP (Sigma-Aldrich® PVP K-30) is chosen as the matrix, and GNPs (TANFENG®, thickness: ~1 nm, diameter: ~50 μm, SSA: ~1200 m^2/g, and purity: >99 wt.%) as the modified nanofillers to form conductive pathways in CPCs. CPCs thus-produced are dispersed in 20 ml ethanol (Honeywell® 24194). The solution is magnetically stirred at 500 rpm at an ambient temperature (25 °C) for 2 h, followed with sonication-assisted dispersion (Brandson® 5800 Ultrasonic Cleaner, 40 kHz) for 1 h, to facilitate uniform and even dispersion of GNPs in PVP. 10 ml DI-water is added to augment the condensation point of solvent to circa -42 °C [41].

To determine the percolation threshold of CPCs, different GNPs-to-PVP mass ratios, varying from 4.0 to 8.0 wt.%, are investigated, respectively. The electrical resistance (ER) of CPCs is calibrated with a digital graphical sampling multimeter (Keithley® DMM7510). The obtained correlation between GNPs loading and electrical conductivity (σ) of the prepared CPCs is shown in **Fig. S1**. Applying the power-law function linear fitting [34] on Eq. (1), the percolation threshold of the CPCs is determined to be 4.93 wt.%.

Deposition of Nanocomposite Ink on B-stage Epoxy Film

The sensors, measuring 20 × 3 mm^2 each, are fabricated by spraying the aqueous CPCs onto a substrate – a partially pre-cured B-stage epoxy film, using an airbrush (HD-130). The scanning speed of nozzle (5 cm/s), stream pressure (0.35 MPa) and distance of target to nozzle (10 cm) are precisely controlled during the spraying process to warrant a consistent initial resistance of sensor.

To make the substrate, B-stage epoxy is spread on a high temperature-resistant release film (AIRTECH® WL5200B nonperforated peel ply) using a spreader at 80 °C, which is proven effective to reduce the viscosity of the epoxy and prevent uncontrollable pre-curing. The epoxy film thus-produced presents the following attributes: 1) the same material properties as the matrix of CFRPs, to which the sensors are implanted; 2) a strong bonding condition among sensors, carbon fibre prepregs and CNT-film-made wires (to be detailed in sequent section); and 3) high flexibility (therefore adaptive to a curved structure) and customizable sensor thickness. These merits warrant high compatibility and non-invasive attributes of implanted sensors with CFRPs. To limit possible flowing of the epoxy during curing, the epoxy film is partially pre-cured, whereby to minimize the effect of epoxy on morphology of the nanocomposite ink deposited on the substrate. The curing degree of epoxy is determined using the differential scanning calorimetry (DSC) technique (Mettler Toledo® DSC3). The curing degree is defined as the ratio of the evolved heat Q_t till time t to the total released heat Q_{ult} during the entire curing process [42], as

$$\alpha = \frac{Q_t}{Q_{ult}} , \quad \textbf{(3)}$$

The evolved heat flow and corresponding curing degree (α) measured by DSC at 130 °C is shown in **Fig. S2** and **Table S1** exemplarily lists five groups of measurement of α against heating duration.

During deposition of the nanocomposite ink on the substrate, the epoxy film remains active and adhesive, the morphology of which may alter under a thermal load. To evaporate the solvent exhaustively, the epoxy film is treated with a freeze-drying process. **Figure 1** compares the morphology of a series of nanocomposite inks which are deposited on epoxy films processed with different pre-treatments, in which different heating durations are adopted. For comparison, the nanocomposite ink is also deposited on an epoxy film which is not processed with such freeze-drying. It can be observed that the original morphology of the nanocomposite ink deposited on a raw epoxy film without any pre-treatment is not maintained through curing process, as a result of the resin flowing. With an increase in pre-curing degree, deposited nanocomposite ink demonstrates improved deposition quality, and a good morphology sustains when α = 0.4 afterwards. Also noted in **Fig. 1** is that exhaustive evaporation facilitates a precise shaping of the nanocomposite ink on the substrate.

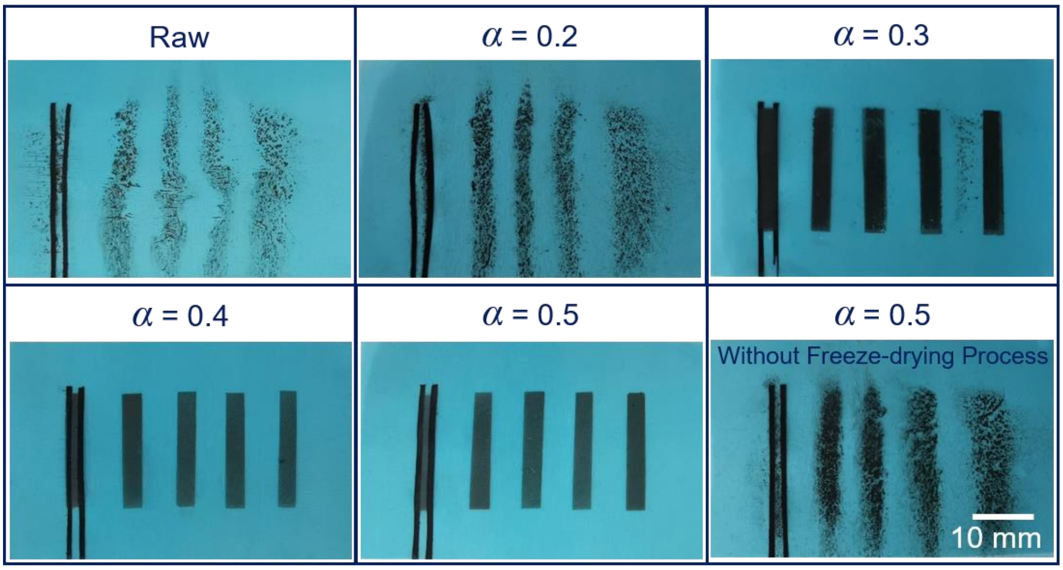

Fig. 1. Comparison of ink deposited-epoxy films processed with different pre-treatments.

Another pre-cured B-stage epoxy film is thus produced, and then placed atop the above epoxy film on which the nanocomposite sensors have already been deposited. Both films, atop and beneath the sensors, respectively called "*upper membrane*" and "*lower membrane*" in what follows, serve as a pair of dielectric membranes, to insulate the sensors from the conductive carbon fibres upon sensor implantation in CFRPs.

Fabrication of CNT-film-made Wires

To further minimize the intrusion to the host composites when sensors (along with associated wires) are implanted, a highly conductive wires is fabricated using CNT-film (DexMat®) made of pure CNTs. The wire is tailored ~1 mm in width and ~10 microns in thickness. With key parameters listed in **Table S2**, the linear resistance of the CNT-film-made wire is only ~20 Ω per meter in length and 1 mm in width, guaranteeing good transmission quality but low intrusion to composites.

Two CNT-film-made wires are aligned along the two opposite edges of each sensor, prior to the encapsulation by the upper membrane. Thus-encapsulated sensors are then fully cured under a vacuum-assisted heating condition (130 °C, 60 min). Notably, different from conventional sensors such as PZT wafers internally embedded in or surface mounted on composites, which are electrified via a pair of electrodes, the vacuum-assisted curing process in this approach imposes a high pressure to indent the CNT-film-made wires into nanocomposite sensors, guaranteeing a good conductive connection but without additional electrodes. Abandoning the conventional electrodes further minimizes the intrusion of the implanted sensors to the host composites.

Lightweight, flexible, small and ultrathin, the fabricated sensors can be deployed in a large quantity in a CFRP structure to configure a dense sensor network. The complete fabrication process of the sensors is illustrated in **Fig. 2**, and sensors produced in their final fashion are pictured in **Fig. 3**.

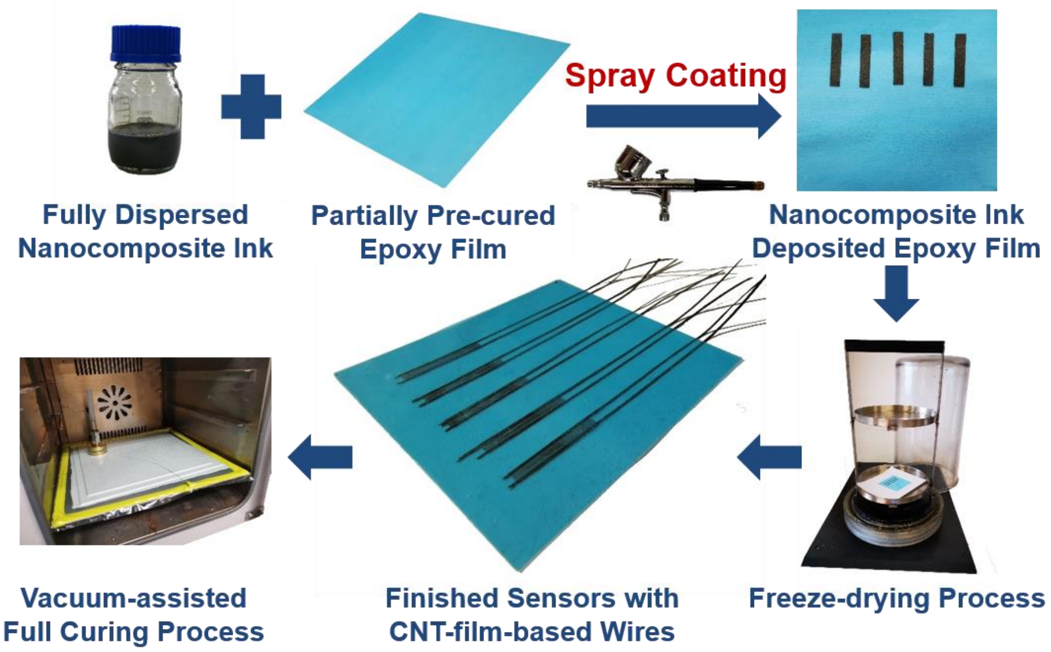

Fig. 2. Flowchart of fabrication process of implantable sensors.

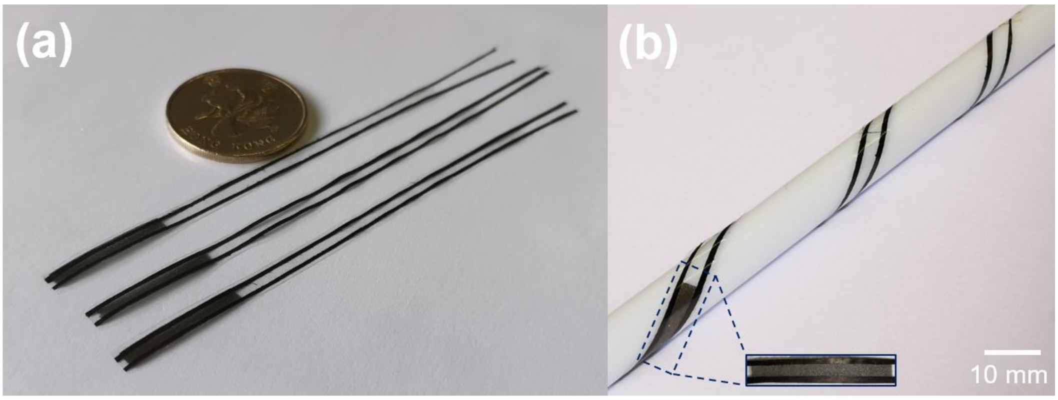

Fig. 3. Photographs of (a) finished nanocomposite sensors with CNT-film-made wires; and (b) sensors showing good flexibility (diameter of the plastic rod in photo: 8 mm).

2.3 Implantation of Networked Sensors into CFRPs

A series of 8-layer quasi-isotropic CFRP laminates of different dimensions, following a stacking sequence of $[0°/90°/45°/-45°]_s$, are made using unidirectional (UD) CF prepregs (Torayca® T300), to each of which the fabricated nanocomposite sensors are implanted to form a sensor network, as schematically illustrated in **Fig. S3**. An industrial-grade autoclaving (Econoclave® EC1.2MX2.4M) curing cycle is followed with key parameters listed in **Table S3.** Upon full curing, the nominal thickness of each CFRP laminate measures 1.15 mm approximately. Each laminate is then trimmed using a water jet cutter (OMAX® PROTOMAX).

2.4 Morphological Characterization

To gain an insight into the nanoscale morphology of the fabricated nanocomposite sensors and the microscopic structure of the sensor-implanted CFRP laminate, morphological characterization is performed on a scanning electron microscopy (SEM) platform (TESCAN® Vega 3), with some representative SEM images displayed in **Fig. 4**.

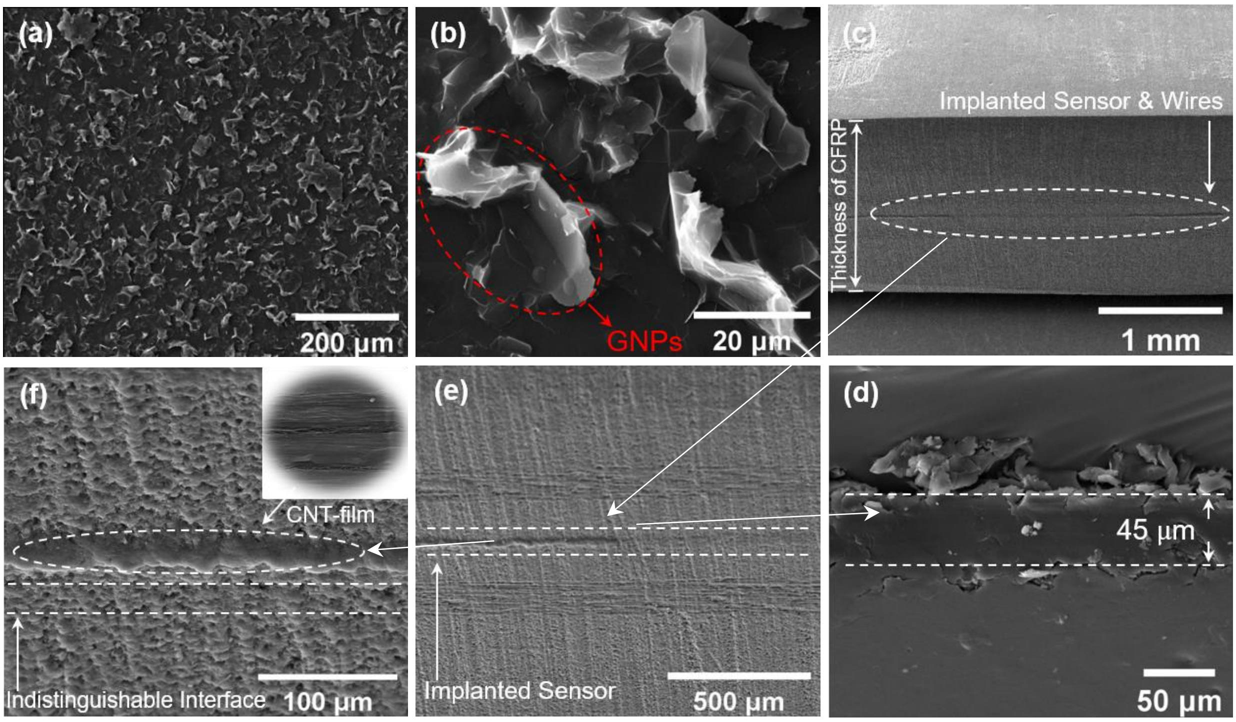

Fig. 4. SEM images of (a, b) GNPs/PVP nanocomposite sensor, at two different scales; (c) cross-sectional view of the CFRP laminate with an implanted sensor and wires; (d) individual implantable sensor; (e) vicinity of the implanted sensor; and (f) the interface between the implanted sensor and host composite.

It is observed in **Fig. 4(a)** that GNPs are dispersed evenly in PVP matrix, and in **Fig. 4(b)** at a smaller scale. The even and uniform distribution of GNPs in PVP is a prerequisite to trigger the tunnel current when a GUW traverses the sensor. **Figure 4(c)** shows the entire cross-section of the CFRP laminate with an implanted sensor with a CNT-film-made wire. The thickness of the implanted sensor including its wire measured in **Fig. 4(d)** is ~45 μm. **Figure. 4(e)** shows the vicinity of the implanted sensor, and at a smaller scale in **Fig. 4(f)**, in both of which it can be noted that the interface between the composite matrix and the sensor (including wire) is obscure, implying a high degree of compatibility of the nanocomposite sensor with CFRPs. The inset of **Fig. 4(f)** shows the SEM image of CNT-film. In conclusion, an ignorable degree of intrusion from implanted sensors and their associate wires to the laminate is noted.

3. Mechanical Properties of CFRP Laminates with Implanted Sensors

To scrutinize possible degradation in mechanical properties of the CFRP laminates due to sensor implantation, two types of mechanical tests – the tensile and flexural tests, are conducted in accordance with ASTM standards. In each type of test, five CFRP laminates, each implanted with a fabricated sensor, are prepared in accordance with the manufacturing procedures as described in Section 2.3, along with another five counterpart laminates of the same dimensions but without any implanted sensor, for comparison.

3.1 Tensile Properties

Quasi-static tensile test is performed to calibrate tensile properties of the laminates (250 × 25 × 1.15 mm^3) and determine their failure modes, according to ASTM D3039. The two ends of each CFRP laminate are immobilized with an aluminium tab using an adhesive (Scotch-Weld® 2216) before tests, to avoid premature failure near the gripping devices. In each laminate implanted with a sensor, the sensor (250 mm × 3 mm × 45 µm) is centralized in the laminate and electrified via two CNT-film-made wires (1 mm wide, and 10 µm thick each), as schematically illustrated in **Fig. 5(a)**. The sensor is positioned between the 4^{th} and 5^{th} plies of each laminate. All laminates are pulled apart on a universal testing system (INSTRON® 5982) with a crosshead speed of 2 mm/min until fracture, and strains are simultaneously recorded by an advanced video extensometer (AVE).

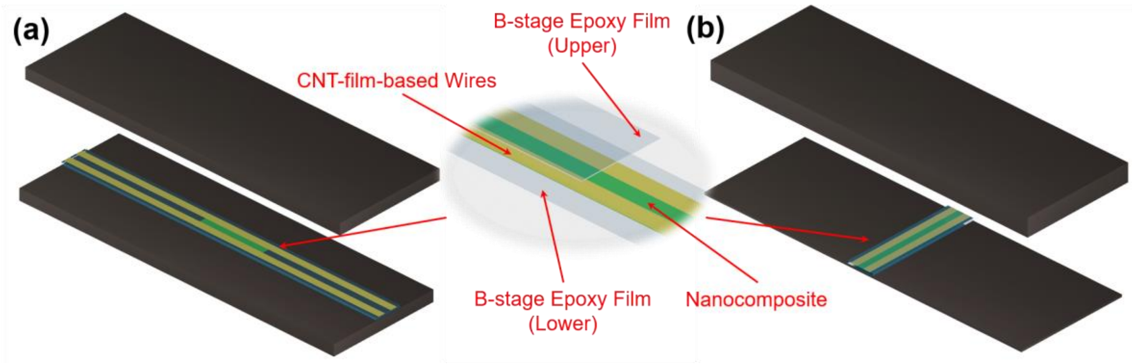

Fig. 5. Schematic illustration of a CFRP laminate implanted with a nanocomposite sensor (with two CNT-film-made wires) for mechanical tests: (a) tensile test; and (b) bending test.

Figure 6 displays the tensile test results of laminates with and without implanted sensors. In **Fig. 6(a),** the obtained stress-strain curves argue that the sensor implantation does not incur observable degradation in elastic attributes of the CFRP laminate, before reaching its ultimate tensile strength (UTS). **Figure 6(b)** compares the averaged UTS and Young's modulus of all laminates with and without sensor implantation, confirming no significant change in between. Only the slight reduction of 2.65% and 1.85% in the tensile strength and in the tensile stiffness, respectively, is observed, attributable to sensor intrusion. In addition, the ignorable degree of standard deviation in test results also proves good consistency in sample manufacturing.

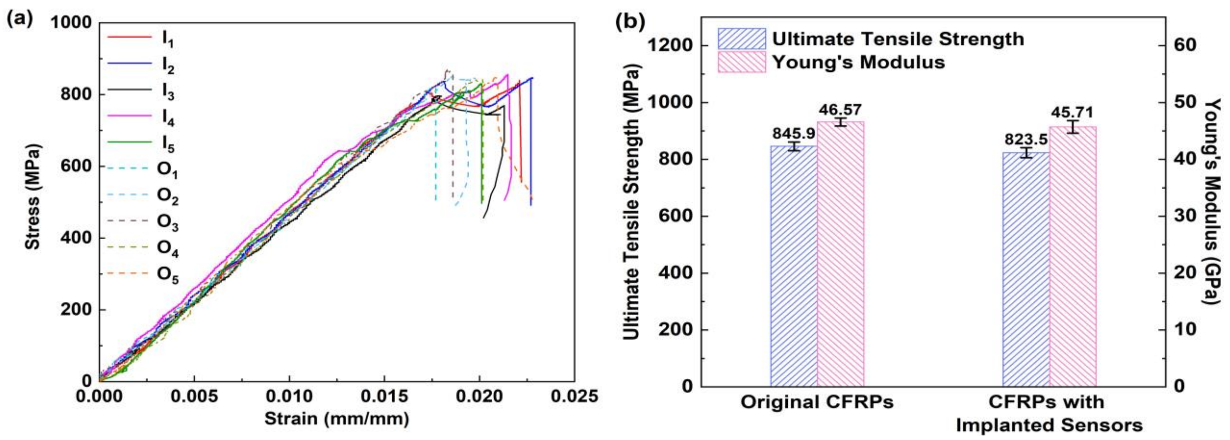

Fig. 6. Results of tensile test: (a) stress-strain curves of CFRPs with and without implanted sensors (I_1-I_5: with implanted sensors; O_1-O_5: without any implanted sensor); and (b) averaged UTS and Young's modulus of laminates with and without sensor implantation.

The failure type of CFRP laminates with and without implanted sensors is identical, in a mixed mode of ply delamination and fibre breakage, as seen in **Fig. 7**. It can be noted in **Fig. 7(a)** and **(b)** that for a laminate with an implanted sensor, the main pathway, along which the delamination is initiated and then progresses, is between the 5th (-45°) and 6th (+45°) plies – analogous to that for those counterpart laminates without sensor implantation as observed in **Fig. 7(c)**. In the figures, the fractured regions manifest strong bonding between the carbon fibre prepreg and the implanted sensor, clarifying that the fracture of the laminate is due to the tensile stress, rather than material degradation at the interface between the implanted sensor and the prepreg.

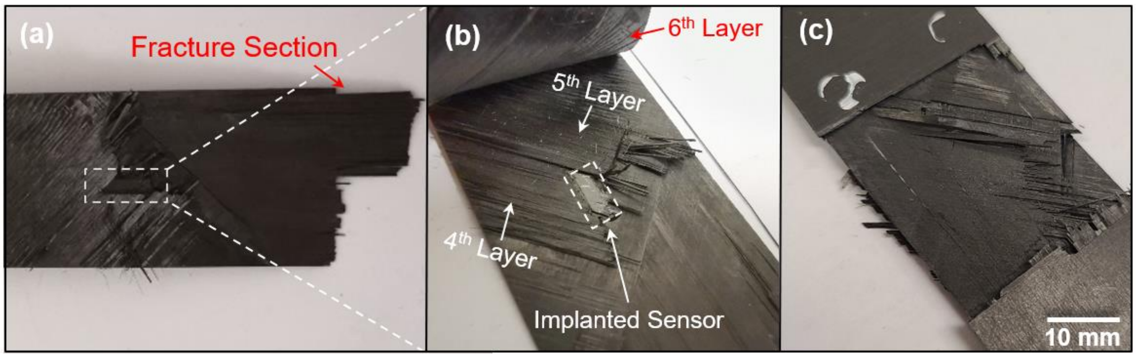

Fig. 7. (a) A fractured laminate with an implanted sensor; (b) the fracture region in (a); and (c) the fracture region of a counterpart laminate without sensor implantation.

3.2 Flexural Properties

Three-point bending test is conducted according to ASTM D790, to comparatively examine the flexural properties of CFRP laminates with and without implanted sensors. Each laminate measures 50.8 × 12.7 × 1.15 mm^3, with a support span of 25.4 mm. A sensor (12.7 mm × 3 mm × 45 μm) with two CNT-film-made wires is implanted at the center of each laminate between the 1st and 2nd plies, at which the maximum normal stress is expected under bending, in **Fig. 5(b)**. The test is also conducted on the universal test platform (INSTRON® 5982) with a crosshead rate of 0.9 mm/min. The maximum normal stress at failure can be determined by **Eq. 4**, while the flexural modulus is calculated using **Eq. 5**, by measuring the slope in the linear region of the load-deflection curve, as

$$\sigma_f = \frac{3PL}{2bd^2}, \tag{4}$$

$$E_B = \frac{L^3 m}{4bd^3}, \tag{5}$$

where σ_f signifies the flexural strength (MPa), *P* the maximum load (N), *L* the support span (mm), *b* the width of the laminate (mm), *d* its depth (mm), E_B the modulus of elasticity in bending (MPa) and *m* the slope of the tangent to the initial straight-line portion of the load-deflection curve.

The obtained flexural properties of the CFRP laminates with and without implanted sensors are compared in **Fig. 8(a)**, to observe nonintrusive effect of an implanted sensor on the flexural properties of a CFRP laminate. The flexural strength of the laminate with an implanted sensor deviates from 916.6 to 950.9 MPa, while flexural modulus decreases marginally from 61.12 to 59.68 GPa. The slight variations in both flexural strength (+3.74%) and modulus (-2.36%) are attributed to the discrepancy in specimen preparation and tests. **Figures 8(b)-(d)** show the fractured laminates under the flexural load, indicating that the failure mode is the compression fracture adjacent to the loading nose, irrespective of implantation of a sensor. The implanted sensor does not initiate a defect, from which the failure develops, outperforming traditional PZT wafers which inevitably reduce the structural integrity to a certain extent [17, 21].

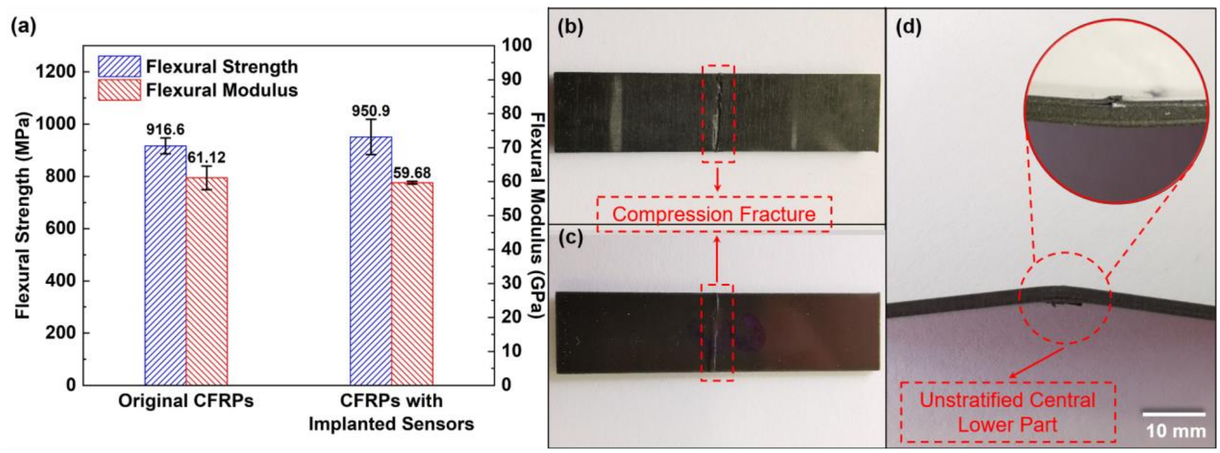

Fig. 8. Results of flexural test: (a) averaged flexural strength and modulus of laminates with and without sensor implantation; fracture region of (b) a counterpart laminate without any implanted sensor; and (c) a laminate with an implanted sensor, with zoomed-in fracture region in (d).

4. Dynamic Response Analysis

With the implanted sensors, dynamic responses of CFRP laminates, when subjected to static load, medium-frequency vibration, and GUWs, respectively, are captured *in situ*.

4.1 Quasi-static Strain

An 8-ply quasi-isotropic CFRP laminate (250 × 25 × 1.15 mm^3) with an implanted sensor placed between the 1st and 2nd plies, is prepared and applied with a quasi-static tensile load, as shown in **Fig. S4**. A digital graphical sampling multimeter (Keithley® DMM7510) measures the change in ER of the implanted sensor via explored CNT-film-made wire ends during the loading process, as depicted in **Figs. S4(b)** and **(c)**. For comparison and calibration, the normal strain at the laminate cross-section, where the sensor is implanted, is measured using the AVE. **Figure 9(a)** presents the obtained stress-strain correlation of the laminate, to observe a linear change in ER prior to yielding. To calibrate the sensitivity of the sensor, a gauge factor (*GF*) is introduced, which reads

$$GF = \frac{\Delta R}{R_0} / \varepsilon \,, \quad \textbf{(6)}$$

where $\Delta R = R - R_0$ (R is the current resistance and R_0 the initial resistance) and ε is the strain. In **Fig. 9**, *GF* is determined to be 34.5 within the elastic regime, which is much higher than that of a commercial strain gauge (~2.0 in general). As seen in **Fig. 9(b)**, $\Delta R/R$ curve is in consistence with the strain curve within the elastic domain, while a large discrepancy is only observed after yielding, which can be attributed to the inconsistency of the effective area for AVE measurement, as seen in **Fig. S4** – AVE measures the strain between the two-gauge points (25 mm) while the implanted sensor reflects the local strain (1 mm gap between two CNT-film-made wires).

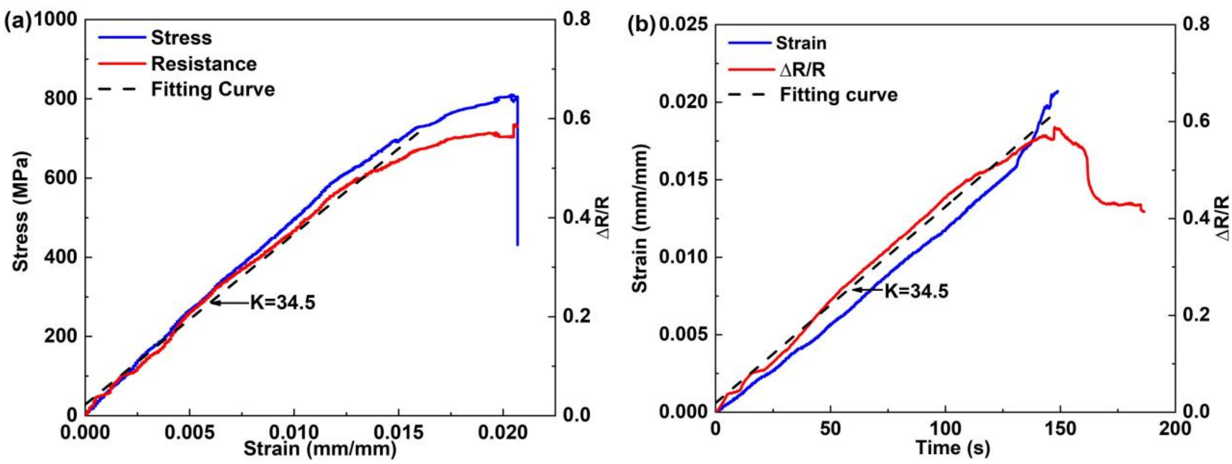

Fig. 9. (a) Stress/ER change *vs.* strain; and (b) strain/ER change *vs.* time under static load.

The piezoresistive behaviour of the nanocomposite sensor manifested during static loading can be interpreted using the sensing mechanism detailed in Section 2.1. When the strain is relatively large in magnitude (in the current case), the variation in contact resistance ($R_{contact}$), due to structural change in the GNP-formed conductive network within the sensor, is dominant over the variation in tunneling resistance ($R_{tunneling}$) and in intrinsic piezoresistivity of GNPs ($R_{Nanoparticle}$).

4.2 Medium-frequency Vibration

The responsivity of a CFRP laminate with an implanted sensor to medium-frequency structural vibration is investigated. An 8-ply quasi-isotropic CFRP laminate (250 × 25 × 1.15 mm^3) with an implanted sensor is prepared, and one end of the laminate is clamped on a dynamic vibration test platform as a cantilever beam, as depicted in **Fig. S5**. The sensor is implanted between the 1^{st} and 2^{nd} plies of the laminate, 150 mm from the clamped end. A commercial strain gauge with the gauge resistance of 120 Ω is surface-glued on the subface (1^{st} ply) of the laminate for calibration. Continuous sinusoidal vibration signals in a sweeping frequency (from 100 to 1000 Hz) are generated with a waveform generator (HIOKI® 7075), to drive a vibration exciter (B&K® 4809) which is in contact with the bottom of the CFRP laminate 35 mm from its free end. Both implanted sensor and the surface-glued strain gauge are linked to a signal acquisition system which consists of a Wheatstone bridge (to convert measured piezoresistive variations to electrical voltage signals), a signal conditioner (KYOWA® CDV-900A) and an oscilloscope (Agilent® DSO9064A).

Bandpass filters are applied to the captured raw signals for screening measurement noise. The processed signals obtained at two typical frequencies, 100 and 1000 Hz, are compared in **Fig. 10**. In **Fig. 10(a)**, waveform distortion and hysteresis are not observed between signals acquired by the implanted sensor and by the surface-glued strain gauge. To take a step further, signals captured by the nanocomposite sensor at 1000 Hz, under different degrees of excitation (4, 6, 8 and 10 V), are compared in **Fig. 10(b)**, to affirm a linear relationship between the magnitude of excitation and the response intensity of the sensors. Here, it is noteworthy that the nanocomposite sensor developed in this study is a sort of piezoresistive sensor, and therefore electrical voltage signals, rather than strain signals, are presented in **Fig. 10**, showing variation in the piezoresistivity measured by the sensor.

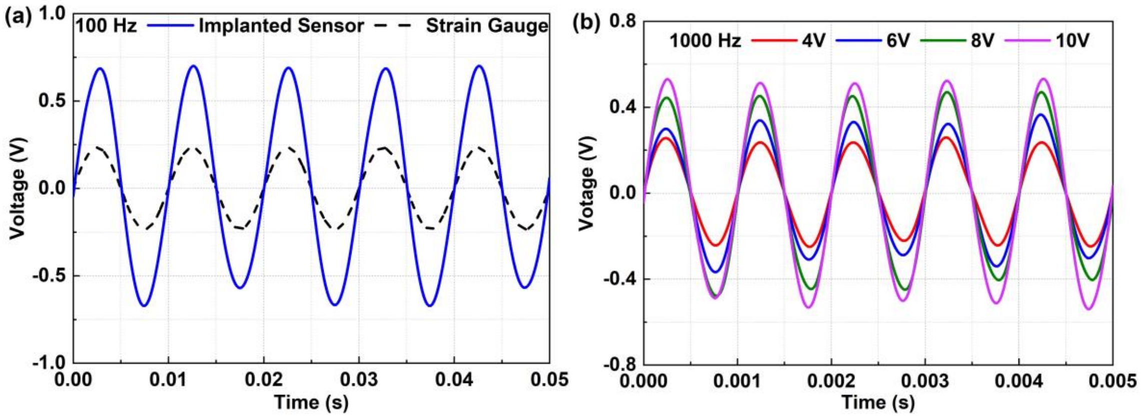

Fig. 10. Responses of CFRPs with an implanted sensor to vibration at (a) 100; and (b) 1000 Hz.

4.3 High-frequency GUWs

To interrogate the responsivity and accuracy of the CFRP laminate with implanted sensors to high-frequency GUWs, an ultrasonic measurement system is configured, shown schematically in **Fig. S6**. An 8-ply quasi-isotropic CFRP laminate (500 × 500 × 1.15 mm^3) which is pre-implanted with a sensor network consisting of four nanocomposite sensors is prepared. The sensor network is implanted between the 4^{th} and 5^{th} plies, with each sensor being 100 mm from an edge, respectively. A miniaturized PZT wafer (PSN-33, Ø: 12 mm, 1 mm thick) is also embedded between the 4^{th} and 5^{th} plies, alongside of an implanted sensor, which simultaneously perceives GUW signals for comparison. To emit a GUW into the laminate, a PZT wafer (PSN-33, Ø: 12 mm, 1 mm thick) is surface-mounted at the center of the laminate. A 5-cycle Hanning-function-modulated sinusoidal toneburst is generated with a waveform generator (configured on a NI® PXIe-10071 platform) and applied on the surface-mounted PZT wafer, amplified to 400 $V_{p\text{-}p}$ via a linear power amplifier (Ciprian® US-TXP-3). The GUW propagation signals are perceived by all implanted sensors and the miniaturized PZT wafer.

All captured signals are pre-averaged 1024 times to minimize measurement uncertainty, and subsequently filtered with a first-order Butterworth filter to mitigate ambient noise. **Figures 11(a)** and **(b)** compare the signals captured by an implanted nanocomposite sensor that is randomly selected from the sensor network and by the PZT wafer, when a GUW is respectively activated at 200 and 450 kHz, as two examples, to observe good coincidence in the arrival time for all the wave modes, including the zeroth-order symmetric Lamb wave mode (denoted by S_0 in the figure), and the zeroth-order anti-symmetric Lamb wave mode (A_0). The discrepancy in signal magnitude is attributed to the different sensing mechanisms of the two types of sensors: the sensing mechanism of the nanocomposite sensor is based on piezoresistivity (tunneling effect) as interpreted in **Section 2.1**, while the PZT wafer measures changes in piezoelectricity. The crosstalk observed in signals at the excitation moment is generated by the linear power amplifier, which does not interfere with signal processing and interpretation.

Across a broad central frequency range from 150 to 450 kHz (with a step of 25 kHz), all the captured signals are pre-averaged 1024 times to minimize measurement uncertainty, filtered with a first-order Butterworth filter to mitigate ambient noise, and consequently processed with a Hilbert transform. Upon signal processing, signal spectra are obtained and shown in **Figs. 11(c)** and **(d)** in a band from 150 to 450 kHz. It shows comparable sensing performance between the implanted sensors and the PZT wafer. Such a sensing capability enables GUW-based SIM for the host composite structure – a difficult task to be fulfilled using conventional nanocomposite piezoresistive sensors [28-34]. In addition, the excitation – a 5-cycle sinusoidal toneburst, is modulated with a Hanning window, so as to constrain the exited wave energy in a narrow band around the excitation frequency (i.e., 200 kHz in this study).

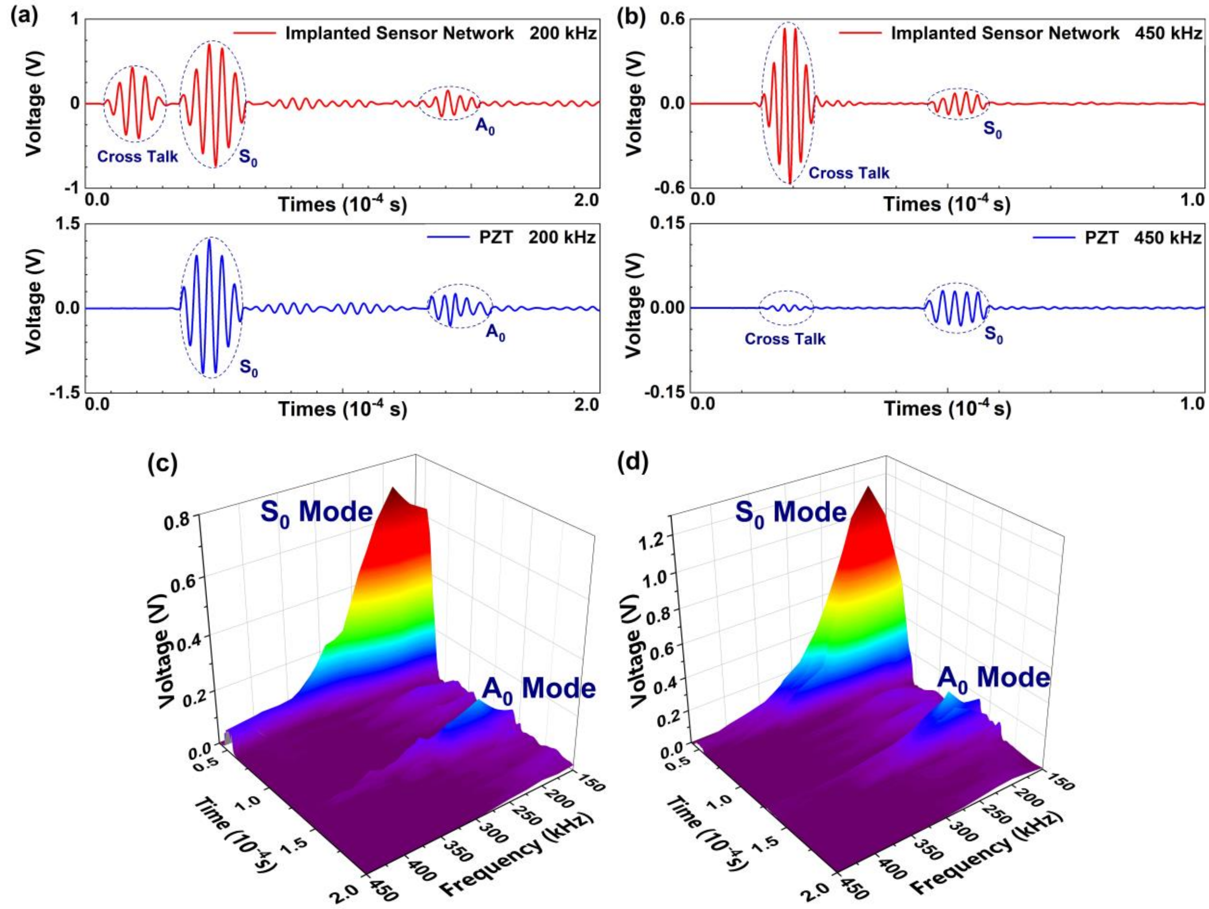

Fig. 11. Signals captured by a nanocomposite sensor randomly selected from the implanted sensor network and by the PZT wafer, at (a) 200 kHz; and (b) 450 kHz; Spectra over time-frequency domain up to 450 kHz, perceived by (c) nanocomposite sensor; and (d) PZT wafer.

5. Conclusion

A new breed of implantable, nanocomposite-based piezoresistive sensor is developed using an additive manufacturing approach (spray coating) with GNPs/PVP-based nanocomposite ink. The sensors are encapsulated by dielectric membranes made of partially pre-cured B-stage epoxy films, and electrified via CNT-film-made wires. Remarkably different from conventional embeddable sensors such as PZT wafers or FBG sensors that unavoidably degrade integrity of the host composites, the developed sensors (including wires), only ~45 μm in thickness, exhibit high compatibility and nonintrusive attributes with the host composites. Comprehensive tensile and bending tests in accordance with ASTM standards demonstrate that the sensors inflict ignorable degradation in mechanical properties of the host composites. With an optimal morphology and based on a quantum tunneling effect-based sensing mechanism, the sensors have a sensing capability to perceive broadband signals *in situ*, ranging from static load-induced strain to structure-guided ultrasonic waves up to 450 kHz – the first time that piezoresistive sensors implanted in CFRPs responds to dynamic strains in such a broad frequency band, outperforming traditional nanocomposite-based piezoresistive sensors which response to low-frequency and large-scale strain only. A gauge factor of 34.5 is achieved for the sensors when used to acquire static load-induced strain. Featuring merits such as lightweight, flexibility and compatibility, the sensors can be densely networked and implanted into CFRPs to implement GUW-based SIM, yet not compromising the composites' original integrity.

Acknowledgments

The work was supported by a General Project (No. 51875492) and a Key Project (No. 51635008) received from the National Natural Science Foundation of China. Z Su acknowledges the support from the Hong Kong Research Grants Council via General Research Funds (Nos. 15202820, 15204419 and 15212417).

References

[1] J. Karger-Kocsis, H. Mahmood, A. Pegoretti, All-carbon multi-scale and hierarchical fibers and related structural composites: A review, Compos. Sci. Technol. 186 (2020) 107932.

[2] J.-H. Kim, P.-S. Shin, D.-J. Kwon, J.-M. Park, 2D Electrical Resistance (ER) Mapping to Detect Damage for Carbon Fiber Reinforced Polyamide Composites under Tensile and Flexure Loading, Compos. Sci. Technol. 201 (2020) 108480.

[3] S. Nonn, … & C. Kralovec, Application of electrical impedance tomography to an carbon fiber-reinforced polymer composite for damage localization, Compos. Sci. Technol. 160 (2018) 231-236.

[4] H. Mei, V. Giurgiutiu, Characterization of multilayer delaminations in composites using wavenumber analysis, Struct. Health Monit. (2020) Paper number: 1475921720939616.

[5] C.M. Yeum, H. Sohn, J.B. Ihn, H.J. Lim, Instantaneous delamination detection in a composite plate using a dual piezoelectric transducer network, Compos. Struct. 94(12) (2012) 3490-3499.

[6] Y. Xiao, W. Qiao, H. Fukuda, H. Hatta, The effect of embedded devices on structural integrity of composite laminates, Compos. Struct. 153 (2016) 21-29.

[7] J.P. Lynch, … & E. Carryer, Design of piezoresistive MEMS-based accelerometer for integration with wireless sensing unit for structural monitoring, J. Aerosp. Eng. 16(3) (2003) 108-114.

[8] P. Dharap, Z. Li, S. Nagarajaiah, E. Barrera, Nanotube film based on single-wall carbon nanotubes for strain sensing, Nanotechnology 15(3) (2004) 379.

[9] C. Kousiatza, … & D. Karalekas, In-situ characterization of 3D printed continuous fiber reinforced composites: A methodological study using FBG sensors, Compos. Sci. Technol. 174 (2019) 134-141.

[10] V.K. Varadan, Wireless microsensors for health monitoring of aircraft structures, MEMS Components and Applications for Industry, Automobiles, Aerospace, and Communication II, International Society for Optics and Photonics, 2003, pp. 175-188.

[11] K.-C. Chuang, C.-C. Ma, C.-K. Chang, Determination of dynamic history of impact loadings using polyvinylidene fluoride (PVDF) films, Exp. Mech. 54(3) (2014) 483-488.

[12] J. Zhu, Y. Wang, X. Qing, A novel electromechanical impedance model for surface-bonded circular piezoelectric transducer, Smart Mater. Struct. 28(10) (2019) 105052.

[13] H. Alnuaimi, U. Amjad, P. Russo, V. Lopresto, T. Kundu, Monitoring damage in composite plates from crack initiation to macro-crack propagation combining linear and nonlinear ultrasonic techniques, Struct. Health Monit. (2020) Paper number: 1475921720922922.

[14] H. Mei, M.F. Haider, R. James, V. Giurgiutiu, Pure S0 and SH0 detections of various damage types in aerospace composites, Compos. B. Eng. 189 (2020) 107906.

[15] M. Lin, F.-K. Chang, The manufacture of composite structures with a built-in network of piezoceramics, Compos. Sci. Technol. 62(7-8) (2002) 919-939.

[16] X. Qing, X. Liu, J. Zhu, Y. Wang, In-situ monitoring of liquid composite molding process using piezoelectric sensor network, Struct. Health Monit. (2020) Paper number: 1475921720958082.

[17] C. Andreades, P. Mahmoodi, F. Ciampa, Characterisation of smart CFRP composites with embedded PZT transducers for nonlinear ultrasonic applications, Compos. Struct. 206 (2018) 456-466.

[18] Y. Liao, P. Zhou, D. Pan, L.-m. Zhou, Z. Su, An ultra-thin printable nanocomposite sensor network for structural health monitoring, Struct. Health Monit. (2019) Paper number: 1475921719859338.

[19] C. Paget, K. Levin, C. Delebarre, Actuation performance of embedded piezoceramic transducer in mechanically loaded composites, Smart Mater. Struct. 11(6) (2002) 886.

[20] M. Yocum, H. Abramovich, A. Grunwald, S. Mall, Fully reversed electromechanical fatigue behavior of composite laminate with embedded piezoelectric actuator/sensor, Smart Mater. Struct. 12(4) (2003) 556.

[21] H.P. Konka, M. Wahab, K. Lian, The effects of embedded piezoelectric fiber composite sensors on the structural integrity of glass-fiber–epoxy composite laminate, Smart Mater. Struct. 21(1) (2011) 015016.

[22] S. Nag-Chowdhury, … & J. Feller, Non-intrusive health monitoring of infused composites with embedded carbon quantum piezo-resistive sensors, Compos. Sci. Technol. 123 (2016) 286-294.

[23] J. Hernandez, … & T. Tallman, An experimental study on the piezoresistive and mechanical behavior of carbon nanocomposites subject to high-rate elastic loading, Compos. Sci. Technol. (2020) 108285.

[24] E.T. Thostenson, T.W. Chou, Carbon nanotube networks: sensing of distributed strain and damage for life prediction and self healing, Adv. Mater. 18(21) (2006) 2837-2841.

[25] B. Yang, … & K. Yang, Multi-functional interface sensor with IFSS enhancing, interface monitoring and self-healing of GF/EVA thermoplastic composites, Compos. Sci. Technol. 167 (2018) 86-95.

[26] J. Zhang, J. Liu, R. Zhuang, E. Mäder, G. Heinrich, S. Gao, Single MWNT-glass fiber as strain sensor and switch, Adv. Mater. 23(30) (2011) 3392-3397.

[27] H. De Luca, D. Anthony, E. Greenhalgh, A. Bismarck, M. Shaffer, Piezoresistive structural composites reinforced by carbon nanotube-grafted quartz fibres, Compos. Sci. Technol. 198 (2020) 108275.

[28] N. Nguyen, … & R. Liang, In situ curing and out-of-autoclave of interply carbon fiber/carbon nanotube buckypaper hybrid composites using electrical current, Adv. Eng. Mater. 18(11) (2016) 1906-1912.

[29] S. Boztepe, H. Liu, D. Heider, E.T. Thostenson, Novel carbon nanotube interlaminar film sensors for carbon fiber composites under uniaxial fatigue loading, Compos. Struct. 189 (2018) 340-348.

[30] P. Zhou, … & Z. Su, An inkjet-printed, flexible, ultra-broadband nanocomposite film sensor for in-situ acquisition of high-frequency dynamic strains, Compos. Part A Appl. Sci. Manuf. 125 (2019) 105554.

[31] Y. Li, … & Z. Su, Acousto-ultrasonics-based health monitoring for nano-engineered composites using a graphene-networked sensing system, Struct. Health Monit. (2019) Paper number: 1475921720929749.

[32] Y. Liao, … & L.-m. Zhou, H. Jin, Z. Zhang, Z. Su, Ultrafast response of spray-on nanocomposite piezoresistive sensors to broadband ultrasound, Carbon 143 (2019) 743-751.

[33] F. Duan, Y. Liao, Z. Zeng, H. Jin, L. Zhou, Z. Zhang, Z. Su, Graphene-based nanocomposite strain sensor response to ultrasonic guided waves, Compos. Sci. Technol. 174 (2019) 42-49.

[34] Y. Li, Y. Liao, Z. Su, Graphene-functionalized polymer composites for self-sensing of ultrasonic waves: An initiative towards "sensor-free" health monitoring, Compos. Sci. Technol. 168 (2018) 203-213.

[35] H. Xu, Z. Zeng, Z. Wu, L. Zhou, Z. Su, Y. Liao, M. Liu, Broadband dynamic responses of flexible carbon black/PVDF nanocomposites: A sensitivity study, Compos. Sci. Technol. 149 (2017) 246-253.

[36] P. Zhou, … & L.-m. Zhou, Z. Zhang, Temperature effect on all-inkjet-printed nanocomposite piezoresistive sensors for ultrasonics-based health monitoring, Compos. Sci. Technol. 197 (2020) 108273.

[37] J. Zhao, G. Wang, R. Yang, X. Lu, M. Cheng, C. He, G. Xie, J. Meng, D. Shi, G. Zhang, Tunable piezoresistivity of nanographene films for strain sensing, ACS Nano 9(2) (2015) 1622-1629.

[38] N. Hu, Y. Karube, C. Yan, Z. Masuda, H. Fukunaga, Tunneling effect in a polymer/carbon nanotube nanocomposite strain sensor, Acta mater. 56(13) (2008) 2929-2936.

[39] J.G. Simmons, Generalized formula for the electric tunnel effect between similar electrodes separated by a thin insulating film, J. Appl. Phys. 34(6) (1963) 1793-1803.

[40] V.K. Shante, S. Kirkpatrick, An introduction to percolation theory, Adv. Phys. 20(85) (1971) 325-357.

[41] Y. Li, J. Yan, L. Qiao, S. Hu, Experimental study on the condensation of ethanol–water mixtures on vertical tube, Heat Mass Transf. 44(5) (2008) 607-616.

[42] W.I. Lee, A.C. Loos, G.S. Springer, Heat of reaction, degree of cure, and viscosity of Hercules 3501-6 resin, J. Compos. Mater. 16(6) (1982) 510-520.